Ocean Engineering 164 (2018) 168–180

Contents lists available at ScienceDirect

Ocean Engineering

journal homepage: www.elsevier.com/locate/oceaneng

Numerical modelling of a steel catenary riser section in the touchdown zone under cyclic loading

Sujan Dutta[a,1], Bipul Hawlader[b,*], Ryan Phillips[c]

[a] Department of Civil Engineering, Royal Military College of Canada, Kingston, Ontario, K7K 7B4, Canada
[b] Department of Civil Engineering, Memorial University, St. John's, Newfoundland, A1B 3X5, Canada
[c] C-CORE, Captain Robert A Bartlett Building, Morrissey Road, St. John's, Newfoundland, A1B 3X5, Canada

ARTICLE INFO

Keywords:
Steel catenary riser
Finite volume method
Soft clay
Cyclic loading
Strength degradation
Suction

ABSTRACT

The fatigue life of steel catenary risers is significantly influenced by cyclic riser–seabed–water interaction in the touchdown zone. In this study, the penetration and extraction of a shallow embedded riser section, subjected to cyclic vertical loading, are simulated using a computational fluid dynamics approach with ANSYS CFX. An empirical strength degradation model is proposed for soil softening due to undrained remoulding and clay–water interaction in the highly sheared interface, termed 'shear wetting.' The combined effects of strain rate and softening on the mobilized shear strength of deepwater offshore clay are implemented in CFX. A sufficiently large number of loading cycles is simulated using this computationally efficient numerical technique to achieve a stable response. A significantly large reduction of vertical resistance of a shallowly embedded riser section due to cyclic loading, as observed in physical model tests, is obtained using the proposed strength degradation model with shear wetting, which cannot be explained simply by undrained remoulding.

1. Introduction

Steel catenary risers (SCRs) — long flexible pipes of typically 150–600 mm diameter — are widely used in deepwater to transport hydrocarbons from seabed well systems to floating platforms or surface vessels. Environmental loading, such as surface waves or currents, causes cyclic motion of the riser. One of the key concerns in the design is the fatigue response of risers near the touchdown point (TDP), the point where the riser first touches the seabed. The fatigue response is significantly influenced by riser–seabed–water interaction in the touchdown zone (TDZ), the zone where cyclic riser–soil interaction exists. In the current industry practice, the fatigue performance is mainly evaluated modelling the seabed as a linear/nonlinear spring or rigid surface. Large-scale field and laboratory tests (e.g., Bridge et al., 2003; Hodder and Byrne, 2010; Wang et al., 2014) and reduced-scale centrifuge tests (e.g., Hu, 2010; Elliott et al., 2013a, b, 2014) were conducted to understand the response of a riser under cyclic loading. Still, this complex behaviour is not well understood.

Environmental loading could cause six degrees of motion; however, the vertical motion of the riser is the most critical because the penetration near the TDP could increase the curvature and bending moment (Clukey et al., 2005). Moreover, suction under the riser during uplift also increases fatigue damage (Clukey et al., 2007; Ting et al., 2010). Therefore, the focus of the present study is to investigate the response of an SCR subjected to cyclic vertical motion only, although it is understood that the response might be influenced by the motions in the other directions in several ways, such as altering trench shape/size and water flow mechanisms.

A riser separates from the seabed near the TDP when lifted upward during cyclic motion. The degree of separation is high during storm events because of the large-amplitude vertical motion. Further away from the TDP in the buried zone, the amplitude of motion reduces and therefore the maximum vertical displacement may not be sufficient to cause separation of the riser from the seabed. Compared to their large-amplitude motion during storm events, risers generally experience much more frequent day-to-day small-to medium-amplitude cyclic motions over a long period, which governs the fatigue design (Bridge, 2005; Clukey et al., 2005, 2007).

Model tests have been conducted to understand riser–seabed–water interaction under cyclic loading. In these tests, the invert of a model pipe section of diameter D is first penetrated into the seabed to the desired depth (w_{in}) and then cyclic vertical displacements of amplitude a are applied. Tests were conducted under the submerged condition in order to investigate the effects of water on vertical resistance. The

* Corresponding author.
E-mail addresses: sd3451@mun.ca (S. Dutta), bipul@mun.ca (B. Hawlader), ryan.phillips@c-core.ca (R. Phillips).
[1] Formerly, Memorial University, St. John's, Newfoundland, A1B 3X5, Canada.

https://doi.org/10.1016/j.oceaneng.2018.06.040
Received 16 November 2017; Received in revised form 30 April 2018; Accepted 13 June 2018

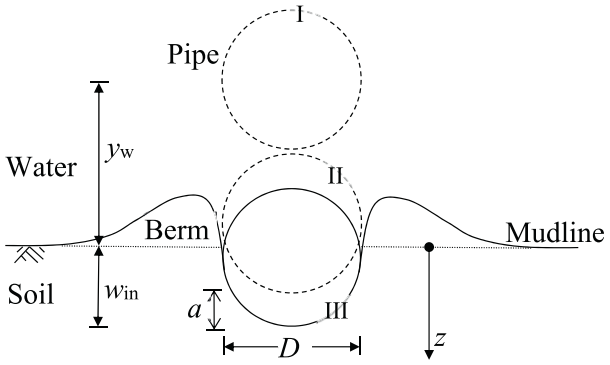

Fig. 1. Problem statement.

depth of embedment (w) represents the vertical distance between the invert of the pipe and mudline (Fig. 1). For brevity, the symbols $\hat{w} = w/D, \hat{w}_{in} = w_{in}/D$ and $\hat{a} = a/D$ are used in the following sections. In most of the tests, cyclic loading started from a shallow initial embedment ($\hat{w}_{in} \leq 1.2$) (Bridge, 2005; Clukey et al., 2005; Aubeny et al., 2008; Langford and Aubeny, 2008a,b; Langford and Meyer, 2010); however, some researchers conducted tests for larger $\hat{w}_{in}$ (Clukey et al., 2008b; Hu et al., 2010; Yuan et al., 2016). When the pipe is not fully covered by soil during cyclic loading, the available 'free water' could interact with seabed sediment at the interface between water and clay.

The following were the key observations in the experimental programs when free water was available. The resistance decreased rapidly with the number of cycles when the pipe/T-bar broke away from the seabed in large-amplitude cyclic motions (Hodder et al., 2008, 2009; Langford and Meyer, 2010; Yuan et al., 2016). A large number of small or medium-amplitude cyclic motions reduced the vertical resistance significantly, even in the tests without pipe/T-bar breakaway (Clukey et al., 2005, 2008b; Ganesan and Bolton, 2013). Soil and free water mixing near the interface exacerbate the strength degradation process. The degradation of vertical resistance in free water cases is much higher than that resulting from undrained remoulding in T-bar tests, when the cyclic motion is applied under a fully embedded condition.

Recognizing the complex nature of riser–seabed–water interaction, mathematical models in the form of a *P-y* curve, where *P* is the vertical resistance per unit length of riser and *y* is the vertical displacement, have been proposed for practical engineering purposes (Bridge et al., 2004; Aubeny and Biscontin, 2009; Randolph and Quiggin, 2009). A number of empirical model parameters are required in these models and the authors proposed the ranges for these parameters based on two-dimensional model test results (Dunlap et al., 1990; Bridge, 2005; Aubeny et al., 2008). The degradation of shear strength due to cyclic loading is not considered in these models. These models have also been used to investigate the fatigue response of risers (e.g., Shiri and Randolph, 2010; Ting et al., 2010; Li and Low, 2011). Nakhaee and Zhang (2010) incorporated the degradation of resistance due to plastic deformation during cyclic loading in the *P–y* curve; however, they neglected the effects of water entrainment, possible erosion and reconsolidation of softened sediment, as reported from physical experiments (Hodder et al., 2013; Sahdi et al., 2017). Aubeny et al. (2015) proposed a revised *P-y* curve where the effects of amplitude and number of loading cycles have been incorporated using a set of empirical equations.

Numerical modelling could provide further insights into the mechanisms and can explain some of these experimental observations. Finite element (FE) simulation of cyclic penetration and extraction processes in a fully embedded (deep) condition is available in the literature (Zhou and Randolph, 2009). Similarly, FE modelling of penetration of a shallowly embedded pipeline has been presented by a number of researchers (Wang et al., 2010; Chatterjee et al., 2012; Dutta et al., 2014). However, numerical modelling of extraction behaviour at shallow depths is very limited. Clukey et al. (2008a) demonstrated some advantages of Eulerian simulations for modelling riser–seabed–-water interaction in the presence of free water. They suggested that soil and free water mixing might be incorporated in the strength degradation model, although it was not considered in that study. Moreover, simulations have been performed only for one loading cycle instead of simulating a sufficiently large number of cycles. Using a finite element limit analysis program, Martin and White (2012) calculated the lower- and upper-bound limit loads of 'wished in place' pipes for rough/smooth and fully-bonded/unbonded cases. The soil has been modelled as rigid-plastic material without softening. Again, cyclic loading was not simulated in that study. The authors of the present study used the Eulerian solution technique in ANSYS CFX to model penetration of a pipe into a soft clay seabed (Hawlader et al., 2015a). They also implemented a simplified strength degradation model as a function of distance from the riser in CFX and simulated only one loading cycle (Hawlader et al., 2015b). Comparing with previous model tests and FE results, it was shown that CFX can simulate both penetration and extraction processes.

In summary, when subjected to cyclic loading, the response of shallowly embedded SCR is very different from the response of a fully embedded T-bar. The numerical modelling of SCR subjected to cyclic displacements near the seabed, where free water could play a major role, is not available. In the present study, numerical simulations in a Eulerian framework are performed using ANSYS CFX software which can accommodate both geotechnical and hydrodynamic aspects of the problem. A soil strength degradation model is proposed and implemented in CFX to simulate the reduction of soil resistance under cyclic loading for a range of model parameters and loading conditions. Using this computationally efficient technique, simulations are continued over a sufficiently large number of cycles.

2. Problem statement

A section of pipe located at a distance y_w above the seabed is displaced downward to $w = w_{in}$ and then a sinusoidal cyclic displacement of amplitude a is applied maintaining an average velocity v_0 during penetration and extraction (Fig. 1). The depth of a soil element from the mudline is z.

3. CFD model development

The general purpose ANSYS CFX 14.0 software is used for numerical modelling (ANSYS CFX, 2012). The computational fluid dynamics (CFD) approach has been used in the past not only for modelling fluid but also for the problems involved in soft seabed sediments including debris flows, glide blocks and out runner blocks modelling (De Blasio et al., 2004a; b; 2005; Gauer et al., 2005, 2006; Harbitz et al., 2003; Zakeri, 2009; Zakeri et al., 2009; Zakeri and Hawlader, 2013). The basic principle of CFD modelling, the similarity and differences between solid mechanics, which is the basis of FE formulations, and the advantages of CFD over FE methods to simulate riser–seabed–water interaction have been discussed in Hawlader et al. (2015a,b).

Fig. 2 shows the CFX model used in the present study. As CFX allows only three-dimensional modelling, the analysis is performed only for one element of 10 mm thickness in the out of plane direction. A riser section of $D = 350$ mm and $L = 10$ mm is placed in water above the seabed at $y_w = 1.0D$. The soil and water domains are discretized into a three-dimensional mesh. Previous FE analyses and model tests for shallow embedded conditions show that the soil elements more than $1.5D$ from the pipe surface do not experience significant deformation during vertical displacement (Dutta et al., 2014). A subdomain of $1.5D$ thickness, the shaded zone in Fig. 2, is created where mesh deformation is not allowed and therefore the size and shape of the mesh in the subdomain do not change with loading. However, mesh distortion is

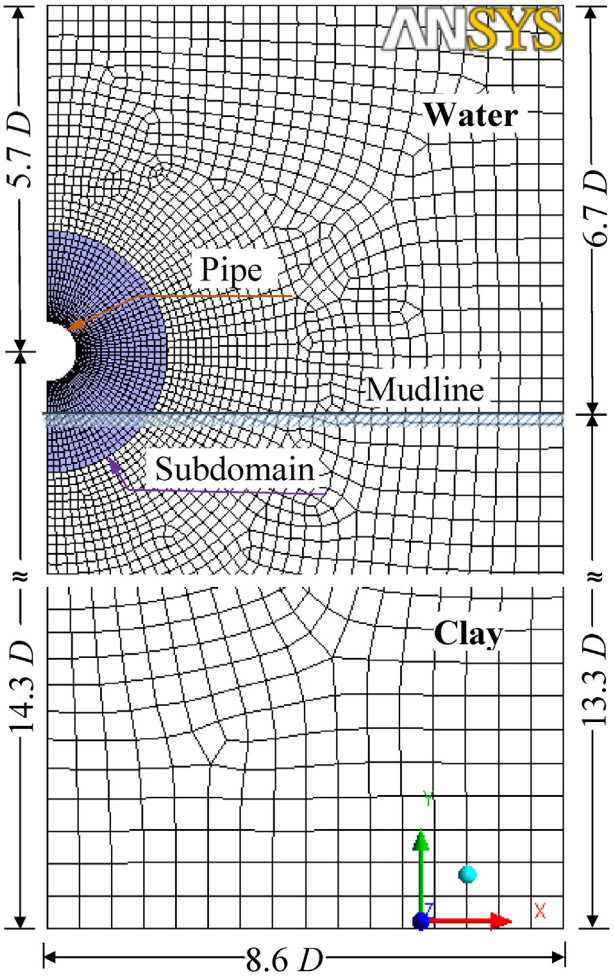

Fig. 2. Model development in CFX.

allowed outside the subdomain. Soil and water, modelled as Eulerian materials, can flow through the mesh both inside and outside the subdomain and also through the outer boundary of the subdomain. Numerical issues related to mesh distortion are avoided using the subdomain. Further details are available in Hawlader et al. (2015, a,b).

All the boundaries are placed at a sufficiently large distance from the riser in order to avoid boundary effects. The bottom and all the vertical boundaries are defined as impermeable surfaces. A no-slip boundary condition is applied to the bottom, which represents zero velocity of soil elements next to this boundary. A free-slip boundary condition is applied to the right vertical face. A symmetry plane boundary condition is applied to the other three vertical faces, which implies that the flow of Eulerian materials (soil/water) on one side of the plane is a mirror image of the flow on the opposite side. The unspecified mesh motion option in CFX is used for the vertical walls. This setting allows the mesh node on these faces to move in the vertical direction, preserving the quality of mesh during the displacement of the riser. The top of the water is defined as an opening to allow water to flow in and out of the domain. Compared with typical FE modelling, the preceding boundary conditions represent rollers in the vertical faces and hinges at the bottom. The mudline is defined by the volume fraction tool in CFX. The volume fraction of water is 1.0 and clay is 0 above the mudline, whereas it is the reverse in the elements below the mudline.

The riser is modelled as an impermeable wall with no-slip boundary condition. Following the concept of the finite-thickness interface element (Supachawarote et al., 2004; Jostad and Andresen, 2004), the shear strength of a thin zone of soil of 10-mm thickness around the riser

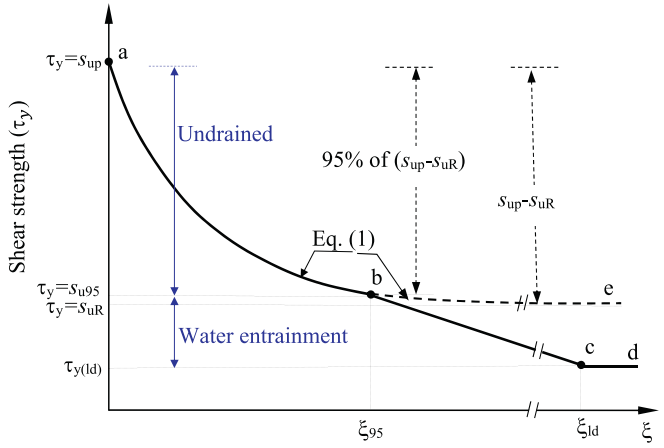

Fig. 3. Shear strength degradation for a given strain rate.

is modelled as $\alpha\tau_y$, where $\alpha = 0$ and $\alpha = 1$ represent the conditions similar to smooth and rough interfaces, respectively, and τ_y is the mobilized shear strength, as discussed below.

4. Shear strength of seabed sediment

The undrained shear strength (s_u) can be used to model soil behaviour if water entrainment does not occur. However, as the behaviour is not undrained when water entrainment occurs, the symbol τ_y is used for mobilized shear strength. Fig. 3 shows the shear strength degradation curve that is used in the present study, where the first segment (*ab*) represents the undrained remoulding of clay. Experimental evidence shows that s_u increases with shear strain rate ($\dot{\gamma}$) and decreases with accumulated plastic shear strain (ξ). Based on the work of Einav and Randolph (2005), the following empirical equation is used for the segment 'ab' in Fig. 3.

$$\tau_y = f_1 f_2 s_{u0} \tag{1}$$

where f_1 and f_2 represent the strain rate and strain softening effects, respectively; s_{u0} is the value of s_u at the reference shear strain rate ($\dot{\gamma}_{ref}$) and prior to any softening. In this study, f_1 and f_2 are defined as (Einav and Randolph, 2005):

$$f_1 = 1 + \mu \log\{\max(\dot{\gamma}, \dot{\gamma}_{ref})/\dot{\gamma}_{ref}\} \tag{2}$$

$$f_2 = \frac{1}{S_t} + \left(1 - \frac{1}{S_t}\right) e^{-3\xi/\xi_{95}} \tag{3}$$

where μ is the rate of change of shear strength per log cycle of $\dot{\gamma}$; remoulded sensitivity $S_t = s_{up}/s_{uR}$ in which s_{up} and s_{uR} are the peak and remoulded values of s_u, respectively, for a given $\dot{\gamma}$; and ξ_{95} is the value of ξ at which s_u is reduced by 95% of (s_{up}-s_{uR}).

Equation (3) successfully simulates the degradation of soil resistance during cyclic vertical movement of cylindrical objects if cycling occurs in fully embedded conditions such as in T-bar tests (Zhou and Randolph, 2009). However, if the cycling occurs near the seabed, the reduction of vertical resistance is significantly higher than that in a fully embedded condition (Clukey et al., 2005; Hodder et al., 2008; Langford and Meyer, 2010). For example, Hodder et al. (2008) showed the reduction of vertical resistance by a factor of 7.5 when cyclic loading was applied at $w_{in} = 0.5D$, whereas the full-flow penetrometer sensitivity was only 2.4. Re-penetration of the riser, which was separated from the seabed during unloading, through the water-filled trench and water entrainment during cyclic loading caused enhanced soil softening. Some experimental investigations show that small-amplitude cyclic motion could also cause a significant reduction of vertical resistance, which is again due to the complex interaction between free water and clay, and cannot be explained simply using undrained remoulding

(Clukey et al., 2005). However, the number of cycles required for a given degree of enhanced softening is higher in small-amplitude motions than in large-amplitude cyclic loadings where the riser has broken away from the seabed.

The experimental results clearly show additional strength reduction in the presence of free water. However, the modelling of free water effects on shear strength degradation is very difficult. A number of factors might be involved in this process including water entrainment, soil-water mixing near the interface, increase in pore water pressure and moisture content, high plastic shear strain accumulation, micro-channel formation and erosion of disturbed soil. Clukey et al. (2008a) noted that the free water effect might be encompassed in an empirical shear strength degradation function, although they did not propose any model or explicitly consider it in numerical modelling. Note that challenges in soil–water interface modelling have been encountered not only for this problem but also in other fields such as riverbed erosion and possible hydroplaning in a submarine debris flow. Conducting a series of laboratory tests for a wide range of initial water content (w) across the soil–fluid transition phase, Boukpeti et al. (2012) proposed an empirical model for shear strength as a power function of w. They also showed that the modelling of shear resistance in a soil mechanics framework better represents the behaviour of this material than fluid mechanics models, for the range of water content they considered.

Following the water entrainment concept of De Blasio and his co-workers for modelling runout of submarine landslides, the strength degradation process is divided into two components (De Blasio et al., 2005; ElverhØi et al., 2005). The first component is due to bond breakage, fabric change and particle alignment, which result from plastic shear strain accumulation (strain softening). This type of undrained remoulding occurs without a significant change in moisture content (e.g. cyclic T-bar tests in a fully embedded condition). The second component of shear strength degradation occurs due to water entrainment in the highly sheared zone near the soil–water interface where free water is available. This process has been termed 'shear wetting' (De Blasio, 2005; ElverhØi et al., 2005). For risers, the effects of water entrainment were examined using centrifuge modelling: both the rate and magnitude soil softening increased significantly when the cyclic displacements were applied to a riser section or penetrometer near the seabed, as compared to softening due to cyclic loading at a fully embedded condition, where only undrained remoulding occurred without free water entrainment (Hodder et al., 2008; Westgate et al., 2013; Yuan et al., 2016). Although it is difficult to quantify accurately, De Blasio (2005) proposed an empirical model for shear strength degradation due to shear wetting as a function of shear strain. Based on some simplifying assumptions, Kobayashi et al. (2015) made an attempt to incorporate water entrainment effects in a modified Cam-Clay based model.

The solid line *abcd* in Fig. 3 shows the shear strength degradation model used in the present study. The line *abe* represents undrained strain softening (Eq. (1)) for a given strain rate. In order to incorporate shear wetting effects, τ_y is linearly decreased from $\tau_y = s_{u95}$ to $\tau_y = \tau_{y(ld)}$ at a large total accumulated shear strain (ξ_{ld}) and then maintained constant (lines *bc* & *cd*). As shown later, large plastic shear strains accumulate mainly near the riser and clay–water interface where shear wetting is also possible. Therefore, the shear wetting effect (segment *bcd*) is primarily applicable to the highly sheared zones near the clay–water interface. In summary, the mobilized shear resistance is calculated as:

$$\tau_y = \begin{cases} f_1\left[\frac{1}{S_t} + \left(1 - \frac{1}{S_t}\right)e^{-3\xi/\xi_{95}}\right]s_{u0} & \text{if } \xi \le \xi_{95} \\ f_1\left[s_{u95} - (s_{u95} - \tau_{y(ld)})(\xi - \xi_{95})/(\xi_{ld} - \xi_{95})\right] & \text{if } \xi_{95} < \xi \le \xi_{ld} \\ f_1\,\tau_{y(ld)} & \text{if } \xi > \xi_{ld} \end{cases} \quad (4)$$

Note that De Blasio (2005) also used an exponential degradation function similar to Eq. (3); however, the strain softening and shear wetting effects have been combined by defining sensitivity as $s_{up}/s_{u(ld)}$. In the present study, these effects are modelled separately (i.e. undrained remoulding at $\xi \le \xi_{95}$ and shear wetting at $\xi > \xi_{95}$) because the mechanisms of strength degradation are different, as discussed. It also has the following advantages. The soil elements far from free water having $0 < \xi \le \xi_{95}$ will experience only undrained remoulding effects. If De Blasio's (2005) type of model is used, these elements will have also some effect of shear wetting, because the strength degradation curve has been defined by $\tau_{y(ld)}$, which is not realistic for riser cyclic motion, as free water is not available. Note that water entrainment could also reduce ξ_{95}; therefore, to capture enhanced soil softening, a reduced value of ξ_{95} has been used to improve the performance of a model for dynamic embedment of pipe near the seabed (Cheuk and White, 2011).

Table 1
Geometry and model parameters used for soil and water in base case analysis.

Diameter of riser (D)	0.35 m
Length of riser section (L)	0.01 m
Average riser velocity (v_0)	0.02 m/s
Initial undrained shear strength of soil (s_{u0})	2.25 kN/m^2
Large-strain shear strength with shear wetting ($\tau_{y(ld)}$)	0.1 kN/m^2
Submerged unit weight of soil (γ')	5 kN/m^3
Interface resistance factor (α)	0.5
Remoulded sensitivity (S_t)	4
Strain softening parameter (ξ_{95})	10
Shear wetting parameter (ξ_{ld})	25
Reference shear strain rate ($\dot{\gamma}_{ref}$)	3×10^{-6} s^{-1}
Shear strain rate parameter (μ)	0.11
Dynamic viscosity of water (μ_{dw})	0.00089 kg/m/s

The geometry and soil parameters used in the 'base case' analysis are shown in Table 1. A uniform τ_y ($= s_{u0}$) of 2.25 kPa is used, although it is understood that s_{u0} might increase with depth in many cases. A typical range of S_t is 2–5 for offshore sediments (Kvalstad et al., 2001). Ranges of ξ_{95} = 10–50 and μ = 0.05–0.2 have been used in the past for successful modelling of undrained remoulding and strain rate effects, respectively (Randolph, 2004; Einav and Randolph, 2005). It is difficult to estimate ξ_{ld} form the results of physical experiments, such as penetrometer cycling, because the effects of water entrainment on overall vertical resistance cannot be separated easily. In the present study, ξ_{ld} = 15–35 and $\tau_{y(ld)}$ = 0.1 kPa are used. Further studies are required for a better quantification of these parameters.

5. Numerical implementation

Both clay and water are modelled as homogeneous multiphase Eulerian materials where the shear behaviour is defined using the dynamic viscosity. For water, a constant value of dynamic viscosity (μ_{dw}) is used (Table 1). Clay is modelled as a visco-plastic non-Newtonian fluid, defining its dynamic viscosity (μ_{ds}) as $\tau_y/\dot{\gamma}$. Using the CFX expression language—a declarative language in CFX for enhanced simulation—the displacement of the riser, material properties and desired output variables are defined.

The CFX does not have any direct option to define shear strength degradation, as shown in Fig. 3. The "additional variable" option in CFX is used to calculate the accumulated shear strain, as required in Eq. (3). In each time increment, $\dot{\gamma}$ is called, which represents the second invariant of the deviatoric strain rate tensor (a scalar quantity). Multiplying $\dot{\gamma}$ by time increment (Δt), the shear strain increment $\Delta\xi$ is calculated. Summing up $\Delta\xi$ over the period of analysis, the accumulated strain ξ is calculated. The authors have developed a special technique in CFX to calculate ξ. Using the value of $\dot{\gamma}$ and ξ, the mobilized shear strength is calculated for each element, which is then used to update μ_{ds}.

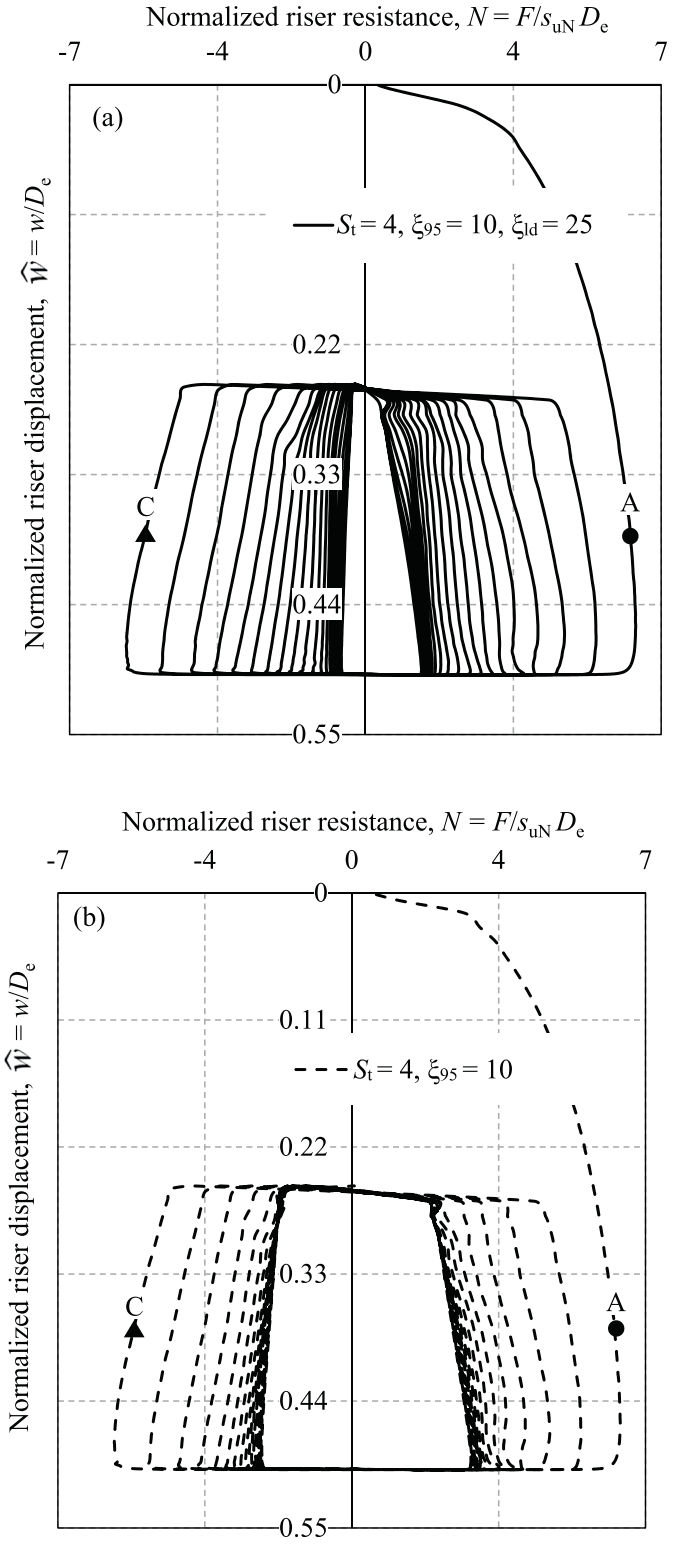

Fig. 4. Calculated normalized resistance: (a) with shear wetting, (b) without shear wetting.

6. Results of base-case analysis

6.1. Penetration and uplift resistance

Fig. 4(a) shows the variation of normalized resistance ($N = F/s_{uN}D_eL$) with normalized depth ($\hat{w} = w/D_e$) for the base case. The undrained shear strength used for normalization (s_{uN}) is $2/\sqrt{3}\ s_{u0}$ (see Hawlader et al. (2015a,b) for further discussion). As finite thickness interface elements and a no-slip riser–soil interface condition are used, the failure occurs in the soil instead of at the riser–soil interface. Therefore, following the concept of Gui and Bolton (1998) and assuming that the failure occurs at a distance of half of the element thickness from the outer surface of the riser, the value of effective diameter (D_e) is calculated as 360 mm (= 350 mm + 2 × 10/2 mm) for 10-mm thick elements just outside the riser.

Fig. 4(a) shows that both the penetration and uplift resistance decrease with the number of cycles (n), although the reduction of N per cycle reduces with an increase in n. Note that, if the extraction is continued instead of re-penetration at $\hat{w} = 0.25$, the uplift resistance will decrease and the riser pipe will be separated from the seabed, leaving a trench in some cases, as observed in model tests (Bridge, 2005) and simulated by the authors in Hawlader et al. (2015b).

The simulation shown in Fig. 4(a) takes only 2.5 h with a 3.4 GHz Intel Core i7 processor and 12 GB RAM. To compare, large deformation FE analysis is performed using Abaqus CEL only for penetration from the seabed to $\hat{w} = 0.5$ (see Dutta et al. (2014) for further details). The present CFX analysis is more than six times faster than Abaqus CEL analysis. The use of a subdomain of fine mesh that moves without any deformation during cyclic motion, together with different solution techniques in CFD, make CFX simulation computationally very efficient.

A similar analysis is performed without shear wetting (i.e. strength degradation is modelled by the line *abe* instead of *abcd* in Fig. 3). Fig. 4(b) shows that both penetration and uplift resistance decrease with n; however, after 6–8 cycles the resistance decreases slowly with cyclic loading, as compared to the shear wetting case. A comparison of Fig. 4(a)–(b) shows that penetration and uplift resistances are the same in both figures for the first few loading cycles because the initial part of the strength degradation curve (segment *ab* in Fig. 3) is the same in both simulations. However, when $\xi > \xi_{95}$, the strength degradation is more in the former case (Fig. 4(a)) with shear wetting (see the vertical distance between lines *be* and *bcd* in Fig. 3). Therefore, the degradation of resistance continues over a large number of cycles in Fig. 4(a) and provides low resistance, as compared to Fig. 4(b).

For a better comparison, the normalized resistance presented in Fig. 4(a)–(b) is plotted against n in Fig. 5. Following Randolph et al. (2007), the values of N at the halfway point of riser travel during cyclic loading (i.e. at $w = 0.375D_e$ in Fig. 4) are obtained (solid circle and triangle in Fig. 4). The obtained penetration and uplift resistance at a

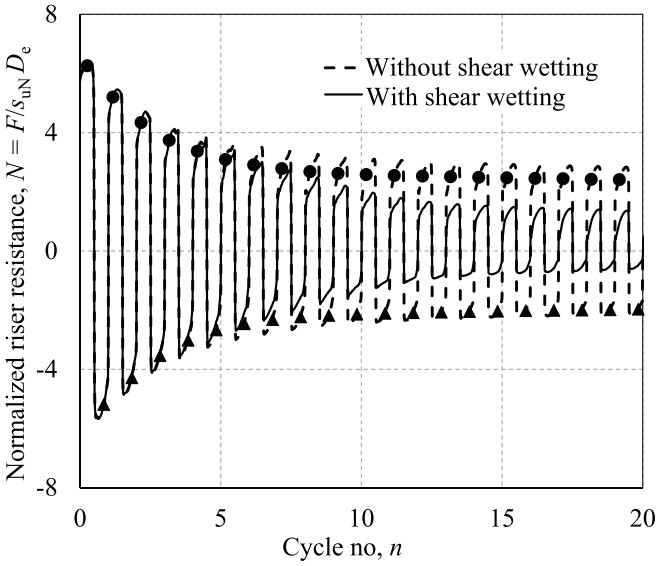

Fig. 5. Comparison of normalized resistance with and without shear wetting.

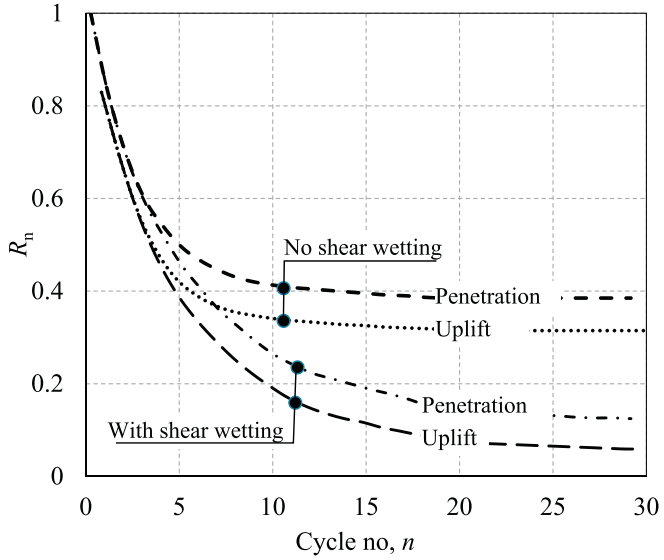

Fig. 6. Degradation of vertical resistance with number of cycles.

given cycle (N_i) are then normalized by the penetration resistance at $w = 0.375D_e$ during initial penetration (point A in Fig. 4), which is denoted as $N_{0.25}$, assuming that 25% of the average total strain that accumulates in the first cycle is developed at this stage (Zhou and Randolph, 2009) and therefore it is considered as $n = 0.25$. Similarly, $n = 0.75$ at $w = 0.375D_e$ during the first uplift (point C in Fig. 4). The degradation of resistance with cyclic loading is then examined by defining the ratio of normalized resistances as $R_n = N_i/N_{0.25}$. The ratio of extraction to penetration resistance for the first cycle ($N_{0.75}/N_{0.25}$) is 0.82, and therefore uplift curves in Fig. 6 start from $R_n = 0.82$. This ratio depends on several factors such as soil properties and loading conditions, as presented in the parametric study. Physical model test results also show a wide variation of this ratio (Bridge et al., 2005; Hodder et al., 2009).

The degradation of vertical resistance is related to soil sensitivity (S_t); however, the sensitivity of soil (S_t) is not equal to $1/R_n$, even at later cycles. For example, Fig. 6 shows that, for the no shear wetting case, $1/R_n$ at $n = 30$ is 2.64 for penetration, which is smaller than S_t (= 4). The following are the main reasons for this difference.

i) Considerable softening occurs prior to mobilization of $N_{0.25}$ that is used to define R_n. For the no shear wetting case in Fig. 6, $N_{0.25}$ is 86% of that in a simulation using a rate-dependent (Eq. (2)) non-softening ($f_2 = 1$) soil model with the other parameters the same as in Table 1.
ii) Strain-rate effects on shear strength increase the vertical resistance. The simulation for the no shear wetting case in Fig. 6 is continued to 65 cycles and it is found that, at $n = 65$, the soil in the failure mechanism is in an almost fully remoulded state ($f_2 \sim 1/S_t$); however, because of strain rate effects ($f_1 > 1$), the mobilized shear strength is greater than the remoulded shear strength.
iii) Self-weight effects (buoyancy) influence the uplift resistance. Simulations with an ideal soil model (rate-independent and non-softening) for $\gamma' = 5\,kN/m^3$ (base case) and $\gamma' \sim 0$ (weightless) show that $N_{0.25}$ for the former case is ~4% higher than that of the latter case.

A similar trend (i.e. $S_t > 1/R_n$) has been reported for full-flow cycling (Yafrate et al., 2009; Zhou and Randolph, 2009). Based on large deformation finite element simulations for $n \leq 6$, Zhou and Randolph (2009) identified three potential reasons for $S_t > 1/R_n$: (i) softening prior to mobilization of $N_{0.25}$, (ii) pipe–soil interface resistance, which they defined as s_{u0}/S_t and (iii) the extent of flow mechanisms outside the fully remoulded zone. These aspects are discussed further in later sections.

6.2. Plastic shear strain

Fig. 7 shows the accumulated plastic shear strain during the 5th, 10th, 15th and 20th cycles just before the end of penetration to $\hat{w} = 0.5$. The figures in the left column (Fig. 7(a–d)) show the results for the no shear wetting case while the right column (Fig. 7(e–h)) is for the shear wetting case. At the 5th cycles, ξ and instantaneous soil velocity vectors are very similar for both cases (Fig. 7(a–e)). The coloured zone in Fig. 7 represents the area where enhanced softening occurs when shear wetting is considered ($\xi > 10$, i.e. $\xi > \xi_{95}$). Comparison between strains in Fig. 7(a)–(e) shows that shear wetting occurs only in a small zone near the pipe (Fig. 7(e)); therefore, the penetration or extraction resistances in $n \leq 5$ are almost the same for both cases (Fig. 6). At $n = 10$, the zone of large ξ is slightly smaller in Fig. 7(f) than that in Fig. 7(b). At these strains, a considerable strength reduction occurs due to shear wetting, and therefore gives low resistance, as compared to the no shear wetting case (Fig. 5). With an increase in n, high shear strains mainly localise near the riser in the shear wetting case, which reduces the strength significantly in that zone. Therefore, in this case, soil elements mainly displace through this narrow zone, as shown by the instantaneous velocity vectors (Fig. 7(g–h)). However, for the no shear wetting case, soil elements displace over a large area (Fig. 7(c–d)).

As the shear strength decreases significantly when shear wetting is considered, this weak soil can displace easily during re-penetration and therefore a higher berm near the riser can be formed, as shown in Fig. 7(g)–(h). However, the berm shape is different when shear wetting is not considered.

The highly softened soil around the riser might be eroded by the flow of this weak soil along the length of the riser during cyclic motion and by the current when it reaches the seabed. These factors, together with lateral movement, could enhance the shear wetting process and trench formation, as observed in the field (Bridge, 2005). The effects of these factors need to be studied further.

6.3. Suction under riser during uplift

The total pressure on a soil element has two components: (i) the ambient water pressure (u_0), which is considered as a reference pressure; (ii) the pressure p that comes from the difference between the density of soil and water and loading during the vertical movement of the pipe. In the numerical simulation, p is calculated in each time increment. When p is less than zero, the total pressure is less than the initial ambient water pressure, which represents the suction. Fig. 8 shows the suction (-ve value of p (< 0)) under the riser during the 5th, 10th, 15th and 20th cycles just before re-penetration at $\hat{w} = 0.25$. The contour intervals of suction are shown in logarithmic scale for clarity. Note that, although cycle numbers are the same as before, because of additional upward displacement of 0.25D, ξ at this stage is higher than the values shown in Fig. 7 but the pattern of ξ is very similar to Fig. 7 and therefore it is not shown again. Instead, the development of suction is examined, which is also an important parameter for design. Comparison of figures in the left and right columns of Fig. 8 shows that suction reduces with the number of cycles when shear wetting is considered. The suction pulls the soil elements down toward the invert of the riser. The extent of zone and magnitude of suction reduce with n in the shear wetting case because of the shear strength reduction with n. However, the reduction is not significant when shear wetting is not considered and therefore a very small change in uplift resistance is calculated after $n = 5$ (Fig. 6). Langford and Meyer (2010) conducted model tests using a 174-mm diameter riser section cycled in highly plastic West African clay where the pore pressure was measured at the invert of the riser. Their test configuration was different from the present study (s_{u0} = 5–7 kPa and cycled between $\hat{w} = 0$ and $\hat{w} = 0.5$);

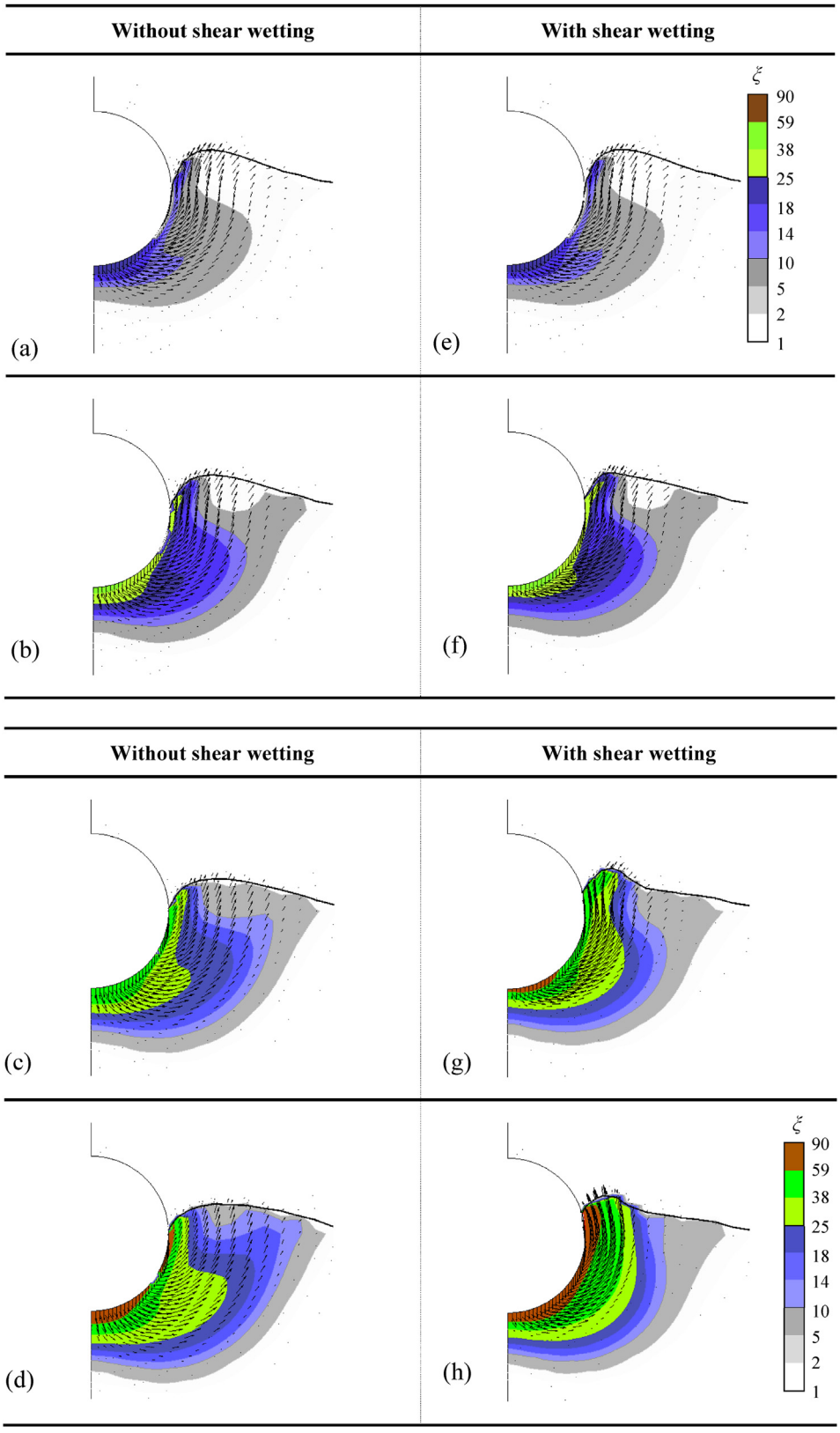

Fig. 7. Plastic shear strain and instantaneous velocity vectors: Left column without shear wetting (a) 5th cycle, (b) 10th cycle, (c) 15th cycle, (d) 20th cycle; Right column, with shear wetting (e) 5th cycle, (f) 10th cycle, (g) 15th cycle, (h) 20th cycle.

however, a negative pore pressure of ~10 kPa at the first cycle and its gradual reduction with the number of cycles were found. This trend is similar to the simulated suction presented in Fig. 8(e)–8(h).

One important observation is that, when shear wetting is considered, a trough above the clay–water interface is formed in the highly softened soil (Fig. 8(f–h)). The size of the trough increases with *n*. During extraction, water gushes toward the trough, as shown by instantaneous velocity vectors of water above the clay–water interface.

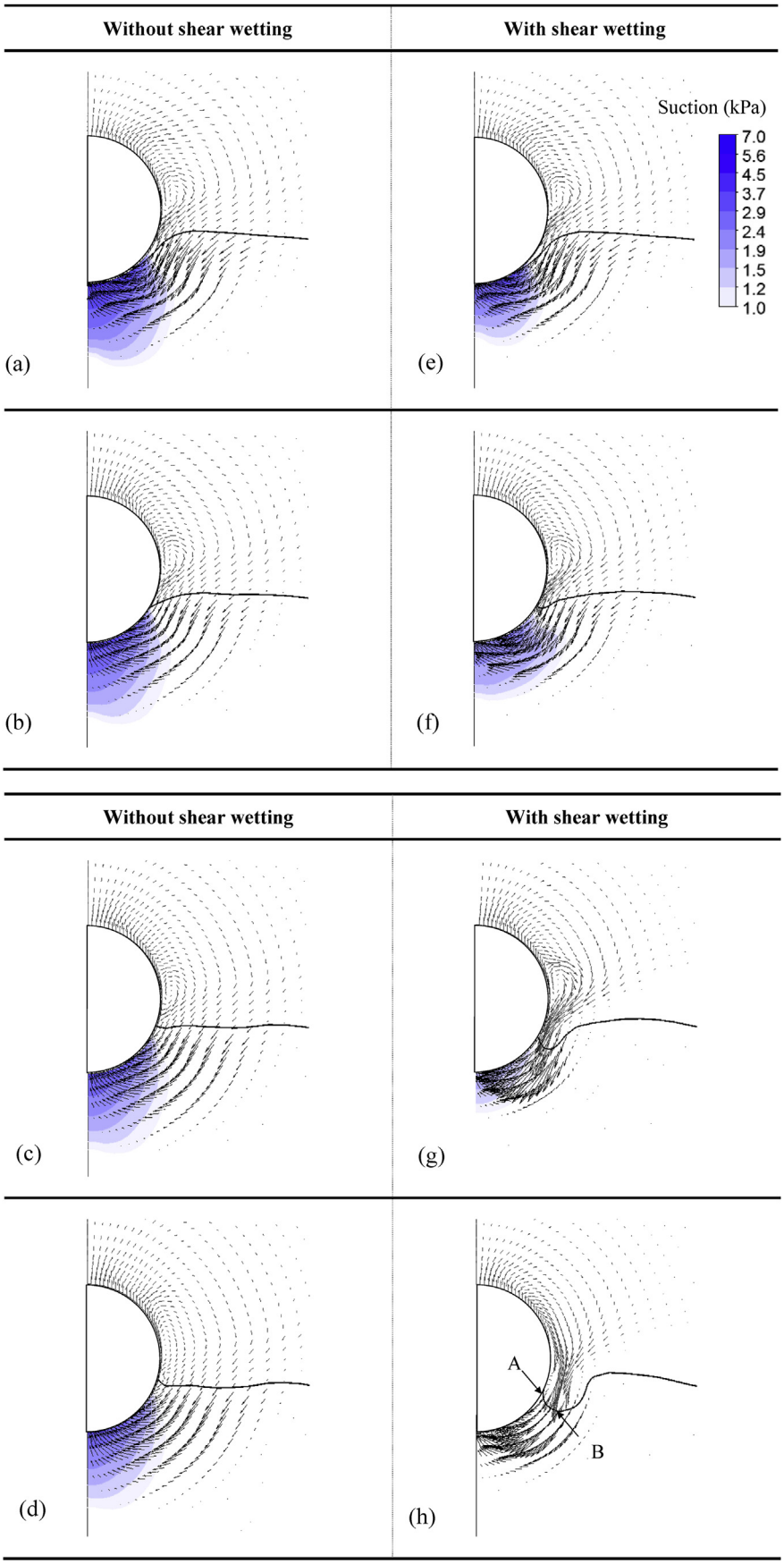

Fig. 8. Mobilization suction and instantaneous velocity vectors during uplift: Left column without shear wetting (a) 5th cycle, (b) 10th cycle, (c) 15th cycle, (d) 20th cycle; Right column, with shear wetting (e) 5th cycle, (f) 10th cycle, (g) 15th cycle, (h) 20th cycle.

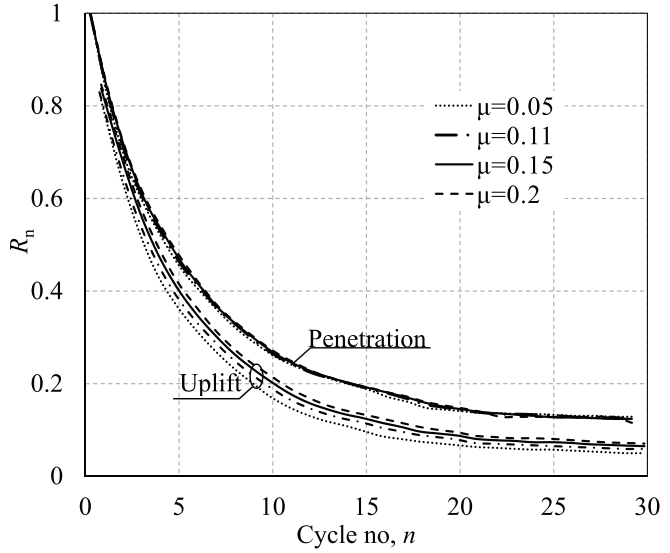

Fig. 9. Effects of strain rate parameter μ on ratio of normalized resistances R_n.

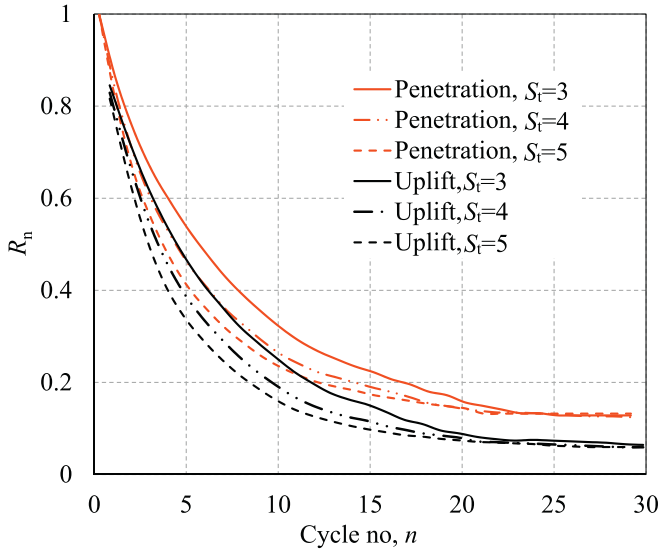

Fig. 10. Effects of soil sensitivity on ratio of normalized resistances R_n.

The bottom of the trough (e.g. point B in Fig. 8(h)) progresses deeper than the highest point of the clay sticks to the pipe surface (point A). Note that, based on experimental observation Clukey et al. (2008a) suggested that during uplift clay might adhere to the riser while failure might occur through the soil. The present simulation with shear wetting can explain that process. When shear wetting is not considered this type of trough does not form (Fig. 8(d)).

7. Parametric study

A parametric study is performed for the shear wetting case, varying only one parameter while the other parameters are the same as in the base case (Table 1).

7.1. Effect of μ

The value of μ could vary between 0.05 and 0.2 (Einav and Randolph, 2005; Lehane et al., 2009). Fig. 9 shows a very small difference between R_n–n curves with μ = 0.05–0.2 for both penetration and extraction resistance. Note, however, that N_i and $N_{0.25}$ increase with μ although their ratio (R_n) is almost the same for all 4 values of μ. For example, $N_{0.25}$ is 6.4 and 7.9 for μ = 0.11 and μ = 0.2, respectively. In summary, μ has a negligible effect on R_n and therefore, R_n is a better parameter to describe cyclic degradation vertical resistance than N_i.

7.2. Effect of S_t

The remoulded sensitivity of offshore clays typically varies between 2 and 5 (Kvalstad et al., 2001; Andersen and Jostad, 2004; Randolph, 2004). As shown in Fig. 3, with an increase in S_t the point b shifts downward, meaning that the shear strength degrades quickly with ξ at the early stage. As a result, both penetration and extraction resistances decrease quickly for a high S_t, as shown in Fig. 10. However, R_n is almost the same for all three values of S_t at a large n. During this stage, significantly high strains generate around the riser (Fig. 7), and therefore the shear strength degrades to $\tau_{y(ld)}$, which is the same for all three cases.

7.3. Effect of ξ_{95}

Fig. 11 shows that R_n decreases quickly with a decrease in ξ_{95} because the lower the value of ξ_{95}, the faster the degradation of strength (Fig. 3). Similar to Fig. 10, R_n is almost the same at large n because the shear strength degrades to $\tau_{y(ld)}$ at this stage near the riser.

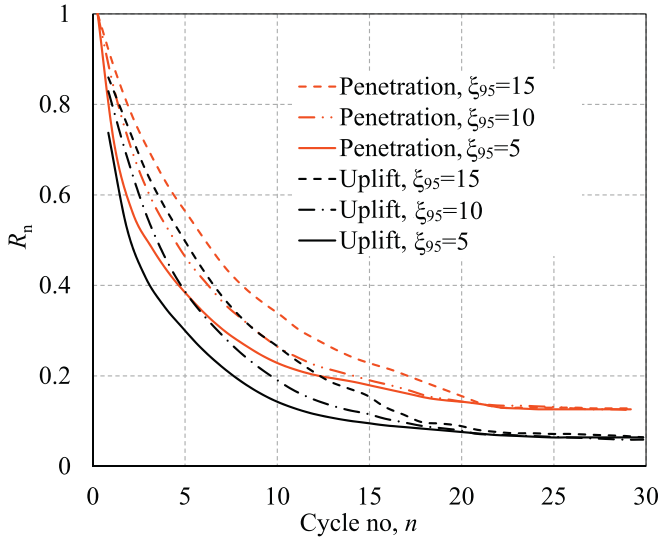

Fig. 11. Effects of strain softening parameter ξ_{95} on ratio of normalized resistances R_n.

7.4. Effect of ξ_{ld}

While S_t and ξ_{95} primarily affect the shape of the initial part of the strength degradation curve ($\xi \le \xi_{95}$), ξ_{ld} mainly influences the latter part at large values of ξ (Fig. 3). Fig. 12 shows that ξ_{ld} does not have a significant influence on R_n up to 4 cycles. However, with an increase in n, the zone of large plastic shear strains ($\xi_{95} < \xi < \xi_{ld}$) around the riser increases where the strength degrades quickly for a small value of ξ_{ld}. Therefore, at a given n (> 4), R_n is smaller for smaller values of ξ_{ld}. Again, R_n will be almost the same for all three values of ξ_{ld} if the analysis is continued for a large number of cycles, because the shear strength in the failure mechanism will degrade to $\tau_{y(ld)}$.

7.5. Effect of initial embedment (w_{in})

Depending upon the location of riser section (with respect to TDP), installation and loading conditions, a section of riser might have different initial depths of embedment and experience cyclic loading of

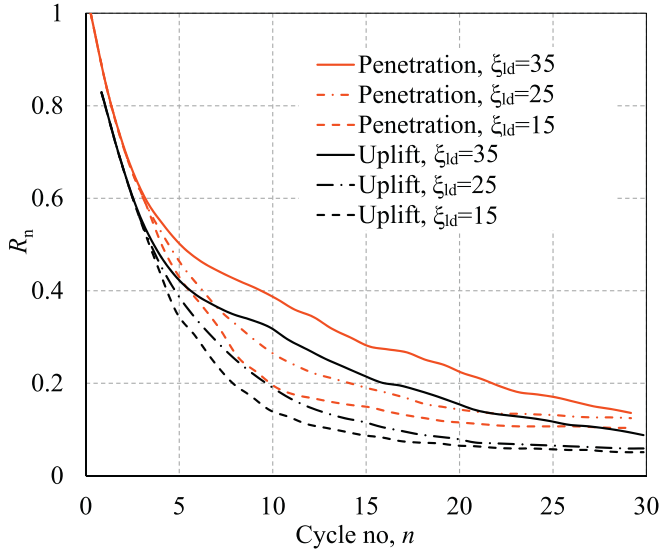

Fig. 12. Effects of strain softening parameter ξ_{ld} on ratio of normalized resistances R_n.

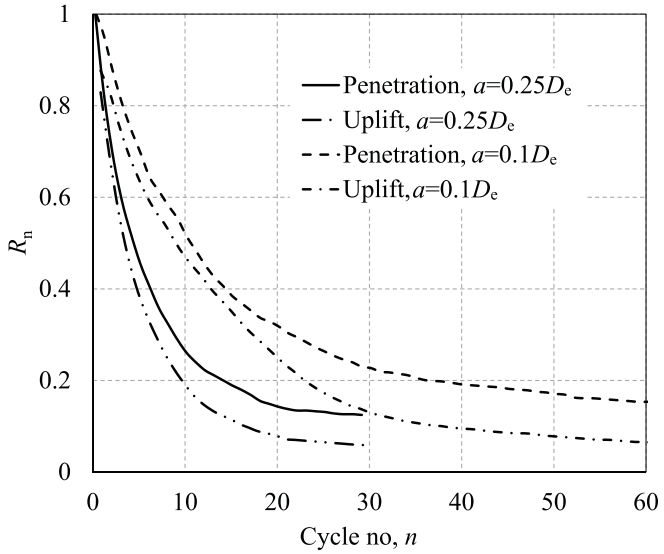

Fig. 14. Effects of cyclic amplitude on ratio of normalized resistances R_n.

different amplitudes.

Fig. 13 shows that R_n decreases quickly with n for shallow initial penetration depths. This trend is similar to the first episode of 20 cycles of Hodder et al. (2009), where they showed that the slope of the load–displacement curve (stiffness) decreases rapidly for a shallow initial embedment. At a large n, the uplift resistance is almost the same for this range of w_{in}, because the localized shear strength of highly softened clay at high ξ mainly governs the extraction behaviour. However, for penetration, R_n in the later cycles increases with an increase in w_{in} because, unlike extraction, the penetration behaviour is also influenced by the less softened clay outside the highly softened zone, and this influence increases for deeper conditions. This has been verified by examining clay velocity vectors at these stages.

7.6. Effect of cyclic amplitude (a)

Experimental evidence shows that small-to large-amplitude riser motion could cause significant degradation of vertical resistance (Clukey et al., 2008b; Hodder et al., 2009; Langford and Meyer, 2010). Fig. 14 shows the variation of R_n with n for two amplitudes ($a = 0.1D_e$ & $0.25D_e$) for $\hat{w}_{in} = 0.5$. Because of higher displacement of the riser in each cycle, R_n decreases quickly with n for $a = 0.25D_e$ and becomes almost constant after $n = 25$. The reduction of R_n with n is slow for the smaller amplitude motion of $a = 0.1D_e$, and the reduction continues right up to 60 cycles. A similar trend of decreasing resistance for small-amplitude motions has been reported from physical model tests (Clukey et al., 2005).

Very large-amplitude motions near the TDP are expected during storm events, although this does not occur frequently. Moreover, the effect of water flow in the trench along the riser is more significant near the TDP. This has not been simulated in the present study.

7.7. Effect of riser–soil interface behaviour

In previous sections, α = 0.5 is used to define the interface elements' shear strength. The effects of α are examined in this section by conducting simulations with two limiting values of α (1.0 for rough and 0.01 for smooth), and these simulations are continued for a large number of cycles ($n = 65$). Fig. 15 shows the variation of R_n, which is calculated using $N_{0.25}$ for the corresponding interface condition. The values of $N_{0.25}$ for rough and smooth conditions are 6.32 and 5.69, respectively. As shown, α does not have a significant influence on the

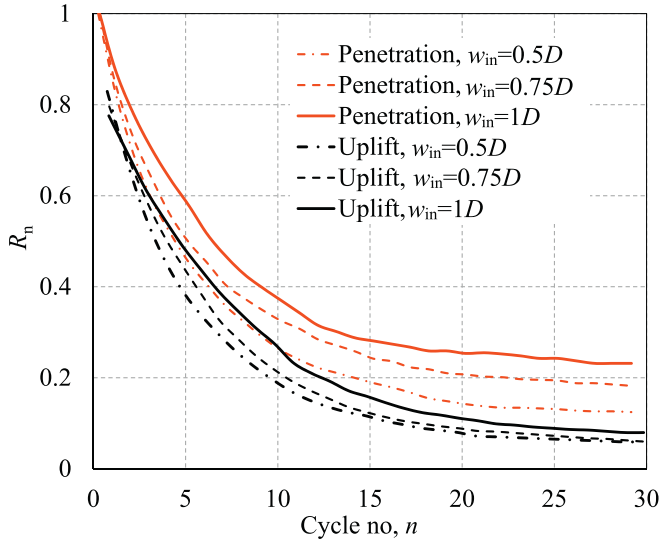

Fig. 13. Effects initial embedment on ratio of normalized resistances R_n.

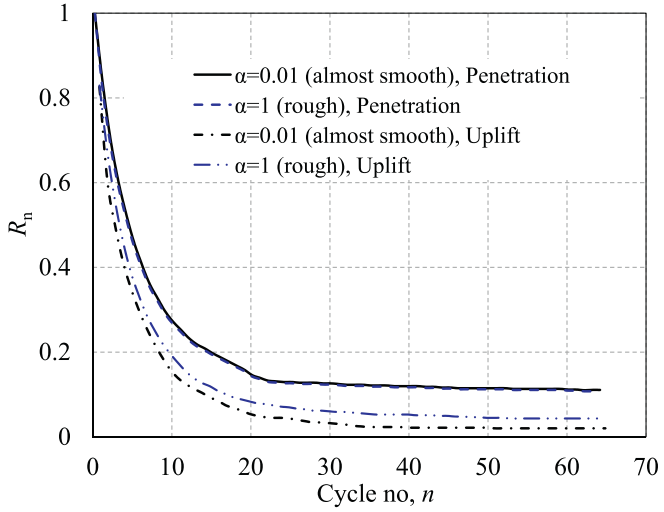

Fig. 15. Effects of riser–soil interface on ratio of normalized resistances R_n.

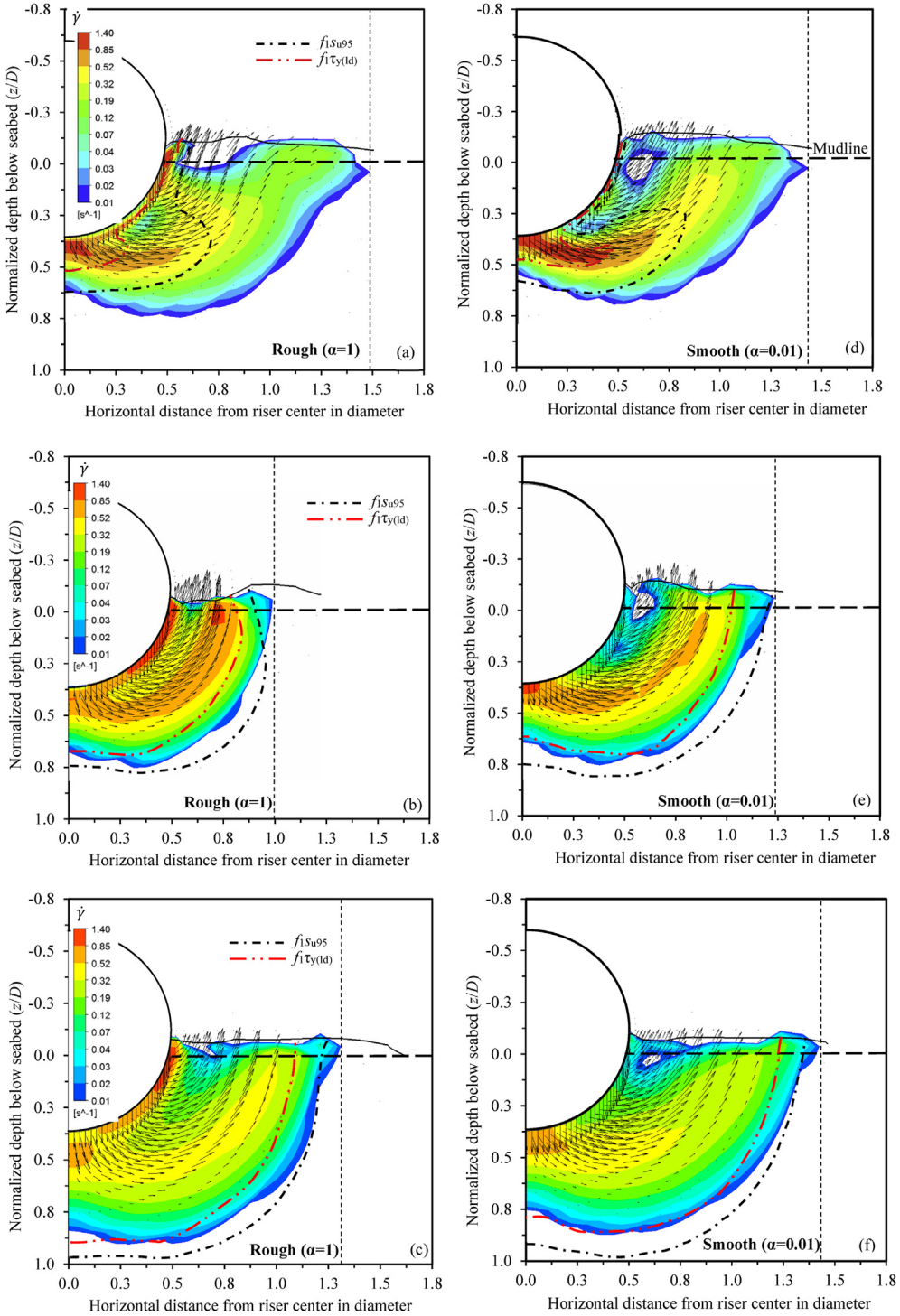

Fig. 16. Soil failure mechanisms at $\hat{w} = 0.375$ during penetration: Left figures for rough interface at (a) 10th cycle, (b) 23rd cycle, (c) 65th cycle; Right figures for smooth interface at (d) 10th cycle, (e) 26th cycle, (f) 65th cycle.

reduction of R_n with the number of cycles.

The extent of soil failure mechanism is presented in Fig. 16, using instantaneous velocity vectors and strain rates, for three different cycles. Drawing two lines in these figures, the level of soil softening in the failure mechanism is divided into three zones: undrained remoulding, shear wetting and large strain shear resistance (i.e. segments ab, bc and cd in Fig. 3). For both interface conditions, the zone of failure mechanism contracts during early cycles and then expands in later cycles. For the rough condition, the lateral extent near the seabed from the centre of the riser is $\sim 1.5D$ at $n = 10$, which is reduced to $\sim 1.0D$ at $n = 26$ and finally increased to $\sim 1.35D$ at $n = 65$ (Fig. 16(a–c)). During early cycles, the shear strength of soil elements near the riser is reduced because of strain-softening, which causes the soil to displace through this softened zone and therefore the extent of the failure mechanism is reduced. However, when a sufficient thickness of soil near the riser is softened to $\tau_{y(ld)}$, the higher strain rate near the riser gives a higher mobilized shear resistance, which causes gradual expansion of the failure mechanism during later cycles. A similar trend is found for the smooth condition (Fig. 16(d–f)) although the extent of the failure mechanism is different. However, it does not have a significant

influence on the reduction of R_n for rough and smooth cases, as shown in Fig. 15.

As discussed, the vertical resistance has two components: (i) soil resistance that acts opposite to the direction of movement of the riser and (ii) buoyancy (acting upward). A number of factors (e.g. the shape of the berm, soil resistance and depth of embedment) influence the buoyancy force (Merifield et al., 2009). In the present study, as the berm size and shape and soil resistance change, the contribution of buoyancy to the vertical resistance varies with cyclic loading and also in the penetration and extraction phases. Moreover, even though the soil underneath the riser moves upward during extraction, the entire failure mechanism is not a true example of a reverse penetration mechanism at the same depth (compare Figs. 7 and 8). In fact, a segment of the riser's surface separates from the soil during extraction (Fig. 8). Because of these two factors (i.e. buoyancy contribution and soil failure mechanism), R_n is smaller in extraction than in penetration. Moreover, the consideration of strain rate increases the vertical resistance. Therefore, $1/R_n$ may not approach $s_{up}/\tau_{y(ld)}$, even after a very large number of cycle.

8. Conclusions

Numerical modelling of the penetration and extraction behaviour of a section of riser subjected to cyclic vertical motion at shallow depths is presented in this study. In order to capture the role of free water in the trench and suction under the riser during extraction, the numerical simulation is performed using a computational fluid dynamics approach with ANSYS CFX software. A strain rate and strain softening dependent model for shear strength of clay is used. In addition to undrained remoulding, the potential effect of water entrainment in the highly sheared zone is incorporated in the shear strength degradation model using the concept of shear wetting. The present CFX model can simulate the flow/large deformation of clay and water around the riser, together with the formation of trench and berm, during cyclic loading. The following conclusions are drawn from this study.

(a) The decrease in vertical resistance primarily occurs during 10–25 cycles of loading and thereafter it occurs slowly. The shear wetting increases the magnitude and rate of reduction of vertical resistance, as compared to that for undrained remoulding only (without shear wetting). The additional reduction of vertical resistance in the shear wetting cases supports experimental observation, and cannot be explained with undrained remoulding only.
(b) When shear wetting is considered, the extent of the soil failure mechanism around the riser reduces in early cycles because of a reduction of the shear strength of the soil that flows through this narrow zone. The failure mechanism then expands with continued cyclic loading. The process of contraction and expansion of the failure mechanism is influenced by riser–soil interface resistance. The enhanced soil softening also causes the reduction of suction under the riser during extraction.
(c) The rate of reduction of the normalized resistance ratio (R_n) with the number of cycles decreases with an increase in initial depth of embedment and increases with cyclic loading amplitude.
(d) The normalized resistance ratio is almost independent of strain rate, although the resistance itself increases with strain rate. The rate of reduction of the normalized resistance ratio with the number of cycles increases with the model parameters that accelerate the soil strength degradation process, such as high sensitivity, low ξ_{95} and low ξ_{ld}.

Finally, although the inclusion of an empirical shear wetting model could better explain the reduction of resistance, as observed in physical experiments, which cannot be explained using the remoulded sensitivity only, the complex process of water entrainment and its effects on shear resistance need to be studied further. Moreover, the effects of a number of factors, such as combined vertical–lateral cyclic motion, as examined through centrifuge modelling (Yuan et al., 2016), erosion of highly softened sediment and its reconsolidation, should be investigated.

Acknowledgements

The work presented in this paper has been supported by the Natural Sciences and Engineering Research Council of Canada, Mitacs, and Petroleum Research Newfoundland and Labrador (PRNL).

Notations

a	cyclic amplitude
D	riser diameter
D_e	effective riser diameter
F	resistance
f_1	strain rate effects
f_2	strain softening effects
L	length of riser section in the out of plane direction
N_i	normalized resistance at ith cycle
$N_{0.25}$	normalized resistance at 0.25 cycle
$N_{0.75}$	normalized resistance at 0.75 cycle
n	number of cycles
R_n	ratio of normalized resistance
s_u	mobilized undrained shear strength
s_{u0}	intact undrained shear strength
s_{up}	peak undrained shear strength
s_{u95}	mobilized shear resistance at ξ_{95}
$\tau_{y(ld)}$	mobilized shear resistance at ξ_{ld}
s_{uN}	$(2/\sqrt{3})s_{u0}$
s_{uR}	remoulded undrained shear strength
S_t	remoulded sensitivity
v_0	riser velocity
w	invert depth of riser from the seabed
w_{in}	initial w
y_w	initial distance from the riser to mudline
z	depth of soil element from mudline
α	riser–soil interface factor
μ	shear strain rate parameter
μ_{ds}	dynamic viscosity of clay
μ_{dw}	dynamic viscosity of water
γ'	submerged soil unit weight
$\dot{\gamma}$	shear strain rate
$\dot{\gamma}_{ref}$	reference shear strain rate
ξ	accumulated absolute plastic shear strain

References

Andersen, K.H., Jostad, H.P., 2004. Shear strength along inside of suction anchor skirt wall in clay. In: Proceedings of the Offshore Technology Conference. Houston, TX, USA, paper OTC 16844.
ANSYS CFX, 2012. CFX Program (Version 14.0) Solver Theory Guide. ANSYS, Canonsburg, PA, USA.
Aubeny, C.P., Biscontin, G., 2009. Seafloor-riser interaction model. ASCE Int. J. Geomech 9 (3), 133–141.
Aubeny, C.P., Gaudin, C., Randolph, M., 2008. Cyclic tests of model pipe in kaolin. Soc. Petroleum Engs 3 (4), 1–6. http://dx.doi.org/10.2118/123131-PA.
Aubeny, C.P., White, T.A., Langford, T., Meyer, V., Clukey, E.C., 2015. Seabed stiffness model for steel catenary risers. In: Proceedings of the 3rd International Symposium on Frontiers in Offshore Geotechnics (ISFOG). Oslo, Norway, pp. 351–356.
Boukpeti, N., White, D.J., Randolph, M.F., Low, H.E., 2012. Strength of fine-grained soils at the solid–fluid transition. Geotechnique 62 (3), 213–226.
Bridge, C., 2005. Effects of Seabed Interaction on Steel Catenary Risers. Ph.D. Thesis. University of Surrey, UK.
Bridge, C., Howells, H., Toy, N., Parke, G., Woods, R., 2003. Full-scale model tests of a steel catenary riser. In: Proceedings of the International Conference of Fluid Structure Interaction. Cardiz, Spain, pp. 107–116.
Bridge, C., Laver, K., Clukey, E., Evans, T., 2004. Steel catenary riser touchdown point vertical interaction models. In: Proceedings of the Offshore Technology Conference. Houston, TX, USA, paper OTC 16628.

Chatterjee, S., Randolph, M.F., White, D.J., 2012. The effects of penetration rate and strain softening on the vertical penetration resistance of seabed pipelines. Geotechnique 62 (7), 573–582.
Cheuk, C.Y., White, D.J., 2011. Modelling the dynamic embedment of seabed pipelines. Geotechnique 61 (1), 39–57.
Clukey, E.C., Haustermans, L., Dyvik, R., 2005. Model tests to simulate riser-soil interaction in touchdown point region. In: Proceedings of the 1st International Symposium on Frontiers in Offshore Geotechnics (ISFOG), pp. 651–658.
Clukey, E., Ghosh, R., Mokarala, P., Dixon, M., 2007. Steel catenary riser (SCR) design issues at touchdown area. In: Proceedings of the 17th International Offshore and Polar Engineering Conference (ISOPE), pp. 814–819.
Clukey, E., Jacob, P., Sharma, P., 2008a. Investigation of riser seafloor interaction using explicit finite element methods. In: Proceedings of the Offshore Technology Conference. Houston, TX, USA, paper OTC 19432.
Clukey, E., Young, A.G., Garmon, G.S., Dobias, J.R., 2008b. Soil response and stiffness laboratory measurements of SCR pipe/soil interaction. In: Proceedings of the Offshore Technology Conference. Houston, TX, USA, paper OTC 19303.
De Blasio, F., Elverhøi, A., Issler, D., Harbitz, C., Bryn, P., Lien, R., 2004a. Flow models of natural debris flows originating from overconsolidated clay materials. Mar. Geol. 213 (1), 439–455.
De Blasio, F., Engvik, L., Harbitz, C., Elverhøi, A., 2004b. Hydroplaning and submarine debris flows. J. Geophys. Res. 109 (C011002), 1–15.
De Blasio, F., Elverhøi, A., Issler, D., Harbitz, C., Bryn, P., Lien, R., 2005. On the dynamics of subaqueous clay rich gravity mass flows–the giant Storegga slide. Norway. Mar. Petroleum Geo 22 (1–2), 179–186.
Dunlap, W.A., Bhojanala, R.P., Morris, D.V., 1990. Burial of vertically loaded offshore pipelines in weak sediments. In: Proceedings of the Offshore Technology Conference. Houston, TX, USA, paper OTC 6375.
Dutta, S., Hawlader, B., Phillips, R., 2014. Finite element modeling of partially embedded pipelines in clay seabed using Coupled Eulerian–Lagrangian method. Can. Geotech. J. 52 (1), 58–72.
Einav, I., Randolph, M.F., 2005. Combining upper bound and strain path methods for evaluating penetration resistance. Int. J. Numer. and Analy. Methods in Geotech. Eng 63 (14), 1991–2016.
Elliott, B.J., Zakeri, A., Macneill, A., Phillips, R., Clukey, E.C., Li, G., 2013a. Centrifuge modeling of steel catenary risers at touchdown zone part I: development of novel centrifuge experimental apparatus. Ocean Eng. 60 (1), 200–207.
Elliott, B.J., Zakeri, A., Barrett, J., Hawlader, B., Li, G., Clukey, E.C., 2013b. Centrifuge modeling of steel catenary risers at touchdown zone part II: assessment of centrifuge test results using kaolin clay. Ocean Eng. 60 (1), 208–218.
Elliott, B., Phillips, R., Macneill, A., Piercey, G., 2014. Physical modelling of SCR in the touchdown zone under three axis motions. In: Proceedings of the 8th International Conference on Physical Modelling in Geotechnics (ICPMG). Perth, Australia, pp. 265–270.
ElverhØi, A., Issler, D., De Blasio, F.V., Ilstad, T., Harbitz, C.B., Gauer, P., 2005. Emerging insights into the dynamics of submarine debris flows. Nat. Hazards Earth Syst. Sci. 5 (5), 633–648.
Ganesan, A.S., Bolton, M.D., 2013. Characterisation of a high plasticity marine clay using a T-bar penetrometer. Underw. Technol. 31 (4), 179–185.
Gauer, P., Kvalstad, T.J., Forsberg, C.F., Bryn, P., Berg, K., 2005. The last phase of the Storegga Slide: simulation of retrogressive slide dynamics and comparison with slide-scar morphology. Mar. Petrol. Geol. 22 (1–2), 171–178.
Gauer, P., ElverhØi, A., Issler, D., De Blasio, F.V., 2006. On numerical simulation of subaqueous slides: back calculations of laboratory experiments of clay rich slides. Nor. J. Geo 86 (3), 295–300.
Gui, M.W., Bolton, M.D., 1998. Geometry and scale effects in CPT and pile design. In: Proceedings of the 1st International Conference on Geotechnical Site Characterization. Atlanta, GA, USA, pp. 1063–1068.
Harbitz, C.B., Parker, G., ElverhØi, A., Marr, J.G., Mohrig, D., Harff, P.A., 2003. Hydroplaning of subaqueous debris flow and glide blocks: analytical solutions and discussions. J. Geophys. Res. 108 (B 7), 1–18.
Hawlader, B., Dutta, S., Fouzder, A., Zakeri, A., 2015a. Penetration of steel catenary riser in soft clay seabed: finite element and finite volume methods. ASCE Int. J. Geomech 15 (6), 1–12.
Hawlader, B., Fouzder, A., Dutta, S., 2015b. Numerical modeling of suction and trench formation at the touchdown zone of steel catenary riser. ASCE Int. J. Geomech 16 (1), 1–14.
Hodder, M.S., White, D.J., Cassidy, M.J., 2008. Centrifuge modelling of riser-soil stiffness degradation in the touchdown zone of a steel catenary riser. In: Proceedings of the 27th International Conference on Offshore Mechanics and Arctic Engineering (OMAE). Estoril, Portugal, pp. 1–9.
Hodder, M.S., White, D.J., Cassidy, M., 2009. Effect of remolding and reconsolidation on the touchdown stiffness of a steel catenary riser: observations from centrifuge modelling. In: Proceedings of the Offshore Technology Conference. Houston, TX, USA, OTC 19871.
Hodder, M.S., Byrne, B.W., 2010. 3D experiments investigating the interaction of a model SCR with the seabed. Appl. Ocean Res. 32 (2), 146–157.
Hodder, M., White, D.J., Cassidy, M.J., 2013. An effective stress framework for the variation in penetration resistance due to episodes of remoulding and reconsolidation. Geotechnique 63 (1), 30–43.
Hu, H.J.E., 2010. Pipeline/riser Soil Interaction Analysis. Ph.D. Thesis. National University of Singapore, Singapore.
Jostad, H.P., Andresen, L., 2004. Modelling of shear band propagation in clays using interface elements with finite thickness. In: Proceedings of the 9th International Symposium on Numerical Models in Geomechanics - NUMOG IX. Ottawa, ON, Canada, pp. 121–128.
Kobayashi, T., Soga, K., Dimmock, P., 2015. Numerical analysis of submarine debris flows based on critical state soil mechanics. In: Proceedings of the 3rd International Symposium on Frontiers in Offshore Geotechnics (ISFOG). Oslo, Norway, pp. 975–980.
Kvalstad, T., Nadim, F., Arbitz, C., 2001. Deepwater geohazards: geotechnical concerns and solutions. In: Proceedings of the Offshore Technology Conference. Houston, TX, USA, OTC 12958.
Langford, T., Aubeny, C., 2008a. Model tests for steel catenary riser in marine clay. In: Proceedings of the Offshore Technology Conference. Houston, TX, USA, OTC 19495.
Langford, T., Aubeny, C., 2008b. Large scale soil-riser model testing on high plasticity clay. In: Proceedings of the 18th International Offshore and Polar Engineering Conference (ISOPE). Vancouver, BC, Canada, pp. 80–86.
Langford, T.E., Meyer, V.M., 2010. Vertical cyclic testing of model steel catenary riser at large scale. In: Proceedings of the 2nd International Symposium on Frontiers in Offshore Geotechnics (ISFOG). Perth, Australia, pp. 803–808.
Lehane, B.M., O'Loughlin, C.D., Gaudin, C., Randolph, M.F., 2009. Rate effects on penetrometer resistance in kaolin. Geotechnique 59 (1), 41–52.
Li, F.Z., Low, Y.M., 2011. Fatigue analysis of a steel catenary riser with uncertain seabed parameters. In: Proceedings of the 30th International Conference on Ocean, Offshore and Arctic Engineering (OMAE). Rotterdam, Netherlands, pp. 1–9.
Martin, C., White, D., 2012. Limit analysis of the undrained bearing capacity of offshore pipelines. Geotechnique 62 (9), 847–863.
Merifield, R.S., White, D.J., Randolph, M., 2009. Effect of surface heave on response of partially embedded pipelines on clay. ASCE J. Geotech. Geoenviron. Eng 135 (6), 819–829.
Nakhaee, A., Zhang, J., 2010. Trenching effects on dynamic behavior of a steel catenary riser. Ocean Eng. 37 (2–3), 277–288.
Randolph, M.F., 2004. Characterization of soft sediments for offshore applications. In: Proceedings of the 2nd International Conference on Site Characterization. Porto, Portugal, pp. 209–232.
Randolph, M., Low, H.E., Zhou, H., 2007. In situ testing for design of pipeline and anchoring systems. In: Proceedings of the 6th International Offshore Site Investigation and Geotechnics Conference: Confronting New Challenges and Sharing Knowledge, London, UK.
Randolph, M., Quiggin, P., 2009. Non-linear hysteretic seabed model for catenary pipeline contact. In: Proceedings of the 28th International Conference on Ocean, Offshore and Arctic Engineering (OMAE). Honolulu, HI, USA, pp. 145–154.
Shiri, H., Randolph, M., 2010. The influence of seabed response on fatigue performance of steel catenary risers in touchdown zone. In: Proceedings of the 29th International Conference on Ocean, Offshore, and Arctic Engineering (OMAE). Shanghai, China, pp. 1–10.
Sahdi, F., White, D.J., Gaudin, C., 2017. Experiments using a novel penetrometer to assess the changing strength of clay during remolding and reconsolidation. ASCE J. Geotech. Geoenviron. Eng 143 (4), 1–7. http://dx.doi.org/10.1061/(ASCE)GT.1943-5606.0001637.
Supachawarote, C., Randolph, M., Gourvenec, S., 2004. Inclined pull-out capacity of suction caissons. In: Proceedings of the 14th International Offshore and Polar Engineering Conference (ISOPE). Toulon, France, pp. 500–506.
Ting, I.H.Y., Kimiaei, M., Randolph, M.F., 2010. Advanced nonlinear hysteretic seabed model for dynamic fatigue analysis of steel catenary risers. In: Proceedings of the 2nd International Symposium on Frontiers in Offshore Geotechnics. Perth, Australia, pp. 833–838.
Wang, D., White, D.J., Randolph, M.F., 2010. Large-deformation finite element analysis of pipe penetration and large-amplitude lateral displacement. Can. Geotech. J. 47 (8), 842–856.
Wang, L., Zhang, J., Yuan, F., Li, K., 2014. Interaction between catenary riser and soft seabed: large-scale indoor tests. Appl. Ocean Res. 45, 10–21.
Westgate, Z.J., White, D.J., Randolph, M.F., 2013. Modelling the embedment process during offshore pipe-laying on fine-grained soils. Can. Geotech. J. 50 (1), 15–27.
Yafrate, N., DeJong, J., DeGroot, D., Randolph, M., 2009. Evaluation of remolded shear strength and sensitivity of soft clay using full-flow penetrometers. ASCE J. Geotech. Geoenviron. Eng 135 (9), 1179–1189.
Yuan, F., White, D.J., O'Loughlin, C.D., 2016. The evolution of seabed stiffness during cyclic movement in a riser touchdown zone on soft clay. Geotechnique 67 (2), 127–137.
Zakeri, A., 2009. Submarine debris flow impact on suspended (free-span) pipelines: normal and longitudinal drag forces. Ocean Eng. 36 (6), 489–499.
Zakeri, A., Hawlader, B., 2013. Drag forces caused by submarine glide block or out-runner block impact on suspended (free-span) pipelines—numerical analysis. Ocean Eng. 67, 89–99.
Zakeri, A., Høeg, K., Nadim, F., 2009. Submarine debris flow impact on pipelines—Part II: numerical analysis. Coast Eng. 56 (1), 1–10.
Zhou, H., Randolph, M., 2009. Numerical investigations into cycling of full flow penetrometers in soft clay. Geotechnique 59 (10), 801–812.